TOPICAL REVIEW — Iron-based high temperature superconductors

Electronic phase diagram of $NaFe_{1-x}Co_xAs$ investigated by scanning tunneling microscopy*

Zhou Xiao-Dong(周晓东), Cai Peng(蔡 鹏), and Wang Ya-Yu(王亚愚)†

State Key Laboratory of Low Dimensional Quantum Physics, Department of Physics, Tsinghua University, Beijing 100084, *China*

(Received 9 May 2013)

Our recent scanning tunneling microscopy (STM) studies of the $NaFe_{1-x}Co_xAs$ phase diagram over a wide range of dopings and temperatures are reviewed. Similar to the high-T_c cuprates, the iron-based superconductors lie in close proximity to a magnetically ordered phase. Therefore, it is widely believed that magnetic interactions or fluctuations play an important role in triggering their Cooper pairings. Among the key issues regarding the electronic phase diagram are the properties of the parent spin density wave (SDW) phase and the superconducting (SC) phase, as well as the interplay between them.

The $NaFe_{1-x}Co_xAs$ is an ideal system for resolving these issues due to its rich electronic phases and the charge-neutral cleaved surface. In our recent work, we directly observed the SDW gap in the parent state, and it exhibits unconventional features that are incompatible with the simple Fermi surface nesting picture. The optimally doped sample has a single SC gap, but in the underdoped regime we directly viewed the microscopic coexistence of the SDW and SC orders, which compete with each other. In the overdoped regime we observed a novel pseudogap-like feature that coexists with superconductivity in the ground state, persists well into the normal state, and shows great spatial variations.

The rich electronic structures across the phase diagram of $NaFe_{1-x}Co_xAs$ revealed here shed important new light for defining microscopic models of the iron-based superconductors. In particular, we argue that both the itinerant electrons and local moments should be considered on an equal footing in a realistic model.

Keywords: iron-based superconductor, scanning tunneling microscopy, spin-density wave, superconductivity

PACS: 74.70.Xa, 74.25.Dw, 74.25.Jb, 74.55.+v **DOI:** 10.1088/1674-1056/22/8/087413

1. Introduction

The high-temperature superconductivity in the iron-based compounds has become one of the most exciting fields in condensed matter physics since it was discovered in 2008.[1] Several key experimental aspects of iron-based superconductors were quickly realized after the discovery of these materials. First, the materials have a quasi-two-dimensional layered structure, with the FeAs or FeSe layer as a common building block. Second, the parent phase has anti-ferromagnetic (AFM) or spin density wave (SDW) order, and superconductivity emerges when the magnetic order is suppressed by chemical doping or pressure. Third, the ground state of the parent compound is metallic, with all five Fe 3d bands crossing the Fermi level (E_F). The first two aspects of iron-based superconductors bear strong similarity to the cuprates. It is especially interesting that the close proximity between the SC phase and the AFM order leads to the postulation that the magnetic interactions or fluctuations are crucial to the paring mechanism. However, the lack of a Mott insulator parent compound suggests that the electron correlation effect in the iron-based systems is not as strong as that in the cuprates. At first glance, this seems to be a relief to the theorists, but on the down side, it makes the choice of theoretical model not so obvious. Both itinerant electron based models that emphasize the Fermiology and local moment based models that emphasize the Mottness have been proposed.[2–6] The multi-band character of the electronic structure also creates extra complexity.

From the experimental point of view, there are still unresolved issues concerning the phase diagram of the iron-based superconductors, such as the nature of the magnetic order in the parent compound, the evolution from the magnetic to the superconducting (SC) phase and the relationship between them, and whether any unexpected new electronic phases exist. Below we elaborate on the current status of these issues.

The parent compound undergoes structural and magnetic transitions as temperature decreases. It changes from the high-temperature tetragonal phase to the low-temperature orthorhombic phase, accompanied by a transition from the paramagnetic phase to the collinear AFM order.[7] By using a local moment Heisenberg Hamiltonian, the spin-wave dispersion in the parent compound can be fitted very well. However, there is another school of thought which adopts an itinerant point of view and ascribes the AFM order to an SDW phase.[8] The mechanism underlying the SDW ordering is the nesting between the hole pocket at the Γ point and the electron pocket at the M point of the Brillouin zone. Therefore, the nature of the

*Project supported by the National Basic Research Program of China (Grant Nos. 2009CB929400 and 2010CB923003).

†Corresponding author. E-mail: yayuwang@tsinghua.edu.cn

© 2013 Chinese Physical Society and IOP Publishing Ltd

magnetic order in the parent compound is still under debate.

Another interesting question is the relationship between the magnetism and superconductivity in the underdoped regime. In the cuprates, the superconductivity sets in only after the AFM order totally disappears. On the contrary, there is an overlap of the AFM order and superconductivity in the underdoped regime in some, if not all, iron-based compounds. Interestingly, the maximum T_c usually occurs near the phase boundary, indicating a close relationship between the AFM order and superconductivity. Hence, a key question here is whether the magnetic order and superconductivity can coexist microscopically or mutually exclude each other.

Another unique physical phenomenon in the iron-based superconductors is the important role of the Hund's rule coupling, which leads to ferromagnetic interaction between the itinerant electrons and local moments.[9] A natural question is whether the interplay between these two degrees of freedom could lead to any unexpected new electronic phases, such as the pseudogap phase in the cuprates and the hidden order phase in the heavy fermions. The exploration of new electronic states in the phase diagram might deepen our understanding of the mechanism of high-T_c superconductivity.

In this review, we will begin with a very brief introduction to the technique of STM and the physics in iron-based superconductors. We mainly focus on the surface problem, and explain why we choose the $NaFe_{1-x}Co_xAs$ system. We then present our STM results in $NaFe_{1-x}Co_xAs$ with varied Co contents all the way from the parent phase to the extremely overdoped non-SC regime.[10,11] The STM results on each distinct phase and their implications will be discussed thoroughly. In the end, we conclude by summarizing the new clues derived from our work and future perspectives from the STM viewpoint.

2. A brief introduction to STM and the iron-based superconductors

The principle of STM is based on the quantum tunneling of electrons across a well-defined vacuum junction. When the tip of STM is brought to close proximity (less than 1 nm) of a conducting sample, a tunneling current I can develop under a certain bias voltage V. Following Bardeen's approach, the tunneling current I can be expressed as

$$I = -\frac{4\pi e}{\hbar}\int_{-eV}^{0} |M_{ts}|^2 \rho_t(\varepsilon)\rho_s(\varepsilon + eV)\,\mathrm{d}\varepsilon.$$

Here, $\rho_t(\varepsilon)$ and $\rho_s(\varepsilon)$ represent the tip's and sample's densities of state (DOS), and $|M_{ts}|$ is the tunneling matrix element, which measures the probability of electrons tunneling between the two electrodes and can be expressed as

$$|M_{ts}|^2 \propto \mathrm{e}^{-2\kappa z}, \quad \kappa = \sqrt{2m\phi}/\hbar.$$

Here, z is the tip-sample distance, m is the electron's mass, and ϕ is the effective tunnel barrier height (usually in a range of 3 eV–5 eV). If we take $\phi = 4$ eV, then I exponentially depends on z with $\kappa \approx 1/\text{Å}$. Therefore, changing z by 1 Å can lead to an order of magnitude change of I, which is the reason that the STM can have atomic scale spatial resolution.

Certain approximations have to be made for realistic STM data analysis. First, we take ρ_t as an energy-independent constant around E_F. A metallic tip made of W or Pt–Ir roughly meets such a requirement. Second, the tunneling matrix element $|M_{ts}|$ is assumed to be independent of the applied bias voltage. This roughly holds when the bias voltage is much smaller than the barrier height, i.e., $eV \ll \phi$. Under these approximations, the expression of I can be simplified into

$$I = -\frac{4\pi e}{\hbar}|M_{ts}|^2 \rho_t \int_{-eV}^{0} \rho_s(\varepsilon + eV)\,\mathrm{d}\varepsilon.$$

In a constant current imaging mode, the tip is scanned on the sample surface with I being a constant through a feedback loop that adjusts z. The recorded $z(x,y)$ is called the topography, and it reflects both the geometric and electronic information of the sample surface. In the scanning tunneling spectroscopy (STS) measurement, we position the tip at a local spot on the sample surface, switch off the feed-back loop, raster the bias voltage V, and record the I (V) curve. Based on the above formula, the derived differential conductance $\mathrm{d}I/\mathrm{d}V$ (V) is proportional to the sample's local density of state (LDOS). Therefore, the STS allows us to probe the evolution of sample's DOS with energy in both the occupied $(V < 0)$ and unoccupied states $(V > 0)$.

Owing to its unique capability of probing the electronic structure at the atomic scale, STM has been applied to cuprate research.[12] Similar to the cuprates, iron-based superconductors have layered structures, so they can be easily cleaved, making them suitable for surface-sensitive probes such as STM and angle-resolved photoemission spectroscopy (ARPES). One should be cautioned that STM is extremely sensitive to surface effects, such as surface reconstruction, surface contamination, or surface charge. Such effects, if not treated properly, hinder the access to intrinsic bulk properties. Therefore, a careful characterization of the cleaved sample surface is required before we draw any conclusion about the sample's bulk electronic properties. Figure 1 shows the schematic crystal structures of four representative iron-based superconductors, the so-called 1111, 122, 111, and 11 series. Most of the reported STM studies have been done on the 122 compounds, because high-quality single crystals are readily available. Take $BaFe_2As_2$ as an example, the crystal will cleave between the Ba and FeAs layers, exposing either the Ba layer or FeAs layer as the top surface. Considering the charge transfer between the Ba layer and FeAs layer in the bulk crystal, the exposed Ba (FeAs) layer would take extra negative

(positive) charge. Such a polar surface is energetically unfavorable and tends to form complex surface reconstructions. As a consequence, there have been numerous reports about various surface topographies of the 122 compounds.[13] Among them the "1×2" and "$\sqrt{2}\times\sqrt{2}$" superstructures are two major types of surface reconstructions.[14–17] There are significant discrepancies on both the surface topography and its chemical identity between results from different groups, and no agreement has been achieved so far. The 1111 series have better surface topography, but also suffer from the polar surface problem. In LaOFeAs, for example, there is charge transfer between the LaO layer and FeAs layer. After the cleavage, the exposed LaO (FeAs) layer is polar and induces a surface electronic state. Our previous STM study on parent LaOFeAs confirms the existence of such a surface state by using the quasiparticle interference (QPI) technique.[18]

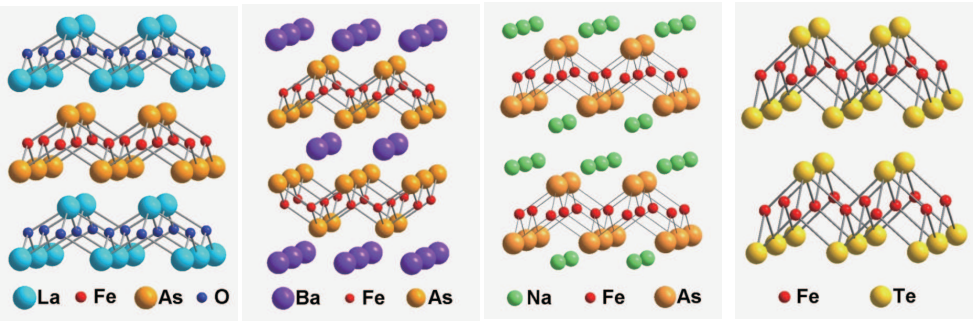


Fig. 1. Schematic crystal structure of four representative iron-based superconductors. All have layered structure, with an FeAs or FeSe layer as a common building block.

The 111 and 11 series compounds turn out to be the ideal systems for STM studies. They both have a mirror symmetric crystal structure. In the 111 NaFeAs (LiFeAs) case, a sample cleaves between two symmetric Na (Li) layers. In the 11 FeSe (FeTe) case, it cleaves between the FeSe (FeTe) layers. The cleaved surface is charge-neutral and devoid of any surface reconstruction, as has been confirmed by recent STM studies.[19,20]

In this work, we choose to study the $NaFe_{1-x}Co_xAs$ system, because it has a phase diagram similar to those of the 1111 and 122 systems (see Fig. 2), and thus can be regarded as a representative iron-based superconductor system.[21] The parent phase has collinear AFM order. Cobalt doping suppresses the AFM order and induces bulk superconductivity, with a possible overlap between the two phases in the underdoped regime. Next we will show the systematic STS studies of the electronic structure across the phase diagram of the $NaFe_{1-x}Co_xAs$ system.

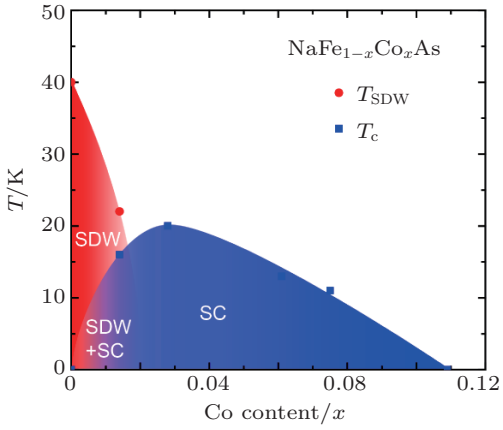


Fig. 2. Schematic electronic phase diagram of $NaFe_{1-x}Co_xAs$ system. The red circles (blue squares) mark the T_{SDW} (T_c) of $NaFe_{1-x}Co_xAs$ studied here. The parent compound has collinear AFM order. Co doping suppresses the AFM order and induces SC. They overlap in the underdoped regime.

3. SDW gap in the parent phase

We first focus on the parent NaFeAs. As mentioned in the introduction, a central debate on the parent phase is the nature of its magnetic ground state. The collinear AFM order can be explained based on a local moment Heisenberg model. For example, in $CaFe_2As_2$, the spin-wave dispersion is fitted well by the J_1–J_2 model, which gives $SJ_{1a} = 49.9\pm9.9$ meV, $SJ_{1b} = -5.7\pm4.5$ meV, and $SJ_2 = 18.9\pm3.4$ meV.[22] Therefore, the nearest-neighbor (NN) exchange coupling along the a and b axes not only changes sign, but also has a very different energy scale. Such a large energy difference between J_{1a} and J_{1b} is unexpected, given the minute lattice distortion. (The difference of the lattice constants along the two axes is less than 1%.) On the other hand, the itinerant SDW picture gains support from the ARPES measured band structure and is consistent with the metallic ground state. However, such a Fermi surface (FS) nesting scenario faces a great challenge in the 11 series compound $Fe_{1+\delta}Te$, whose magnetic order wave vector is rotated 45° relative to the FS nesting wave vector.[23] The recently discovered $A_yFe_{1.6+x}Se_2$ (A = K, Rb, Cs, Tl, etc.)

also challenges the applicability of the itinerant picture. The heavy electron doping in the $A_yFe_{1.6+x}Se_2$ system leaves only four electron pockets at the M point on the FS. However, the FS nesting between electron pockets cannot explain the so-called block-AFM magnetic order found in the system.[24]

NaFeAs undergoes structural and magnetic transitions successively at $T_S = 52$ K and $T_N = 40$ K. Its magnetic order is usually ascribed to an SDW order, which reconciles with the very small magnetic moment ($0.09 \pm 0.04\ \mu_B$) determined by a neutron experiment.[25] An SDW gap opening is also indirectly detected by the infrared optical measurement.[26] However, direct evidence of an SDW gap has yet to be found. The STM can fulfill this task by directly probing the sample's DOS at E_F.

Figure 3(b) displays the spatially-averaged dI/dV spectroscopy taken at $T = 5$ K, which shows that an energy gap opens at E_F. In Fig. 3(a), we show the dI/dV spectra taken at various temperatures. With increasing T, the gap is gradually filled up and closes at $T_N = 40$ K, right at the Neel temperature. Such varied-T measurement unambiguously confirms the SDW origin of the gap found in NaFeAs. The 5 K dI/dV spectroscopy reveals three important features of the SDW gap. First, its line shape is highly asymmetric with respect to E_F, and the gap bottom is not at E_F. Second, there is a large residual DOS at E_F, indicating a partial gap opening on the FS. Third, the gap size defined from the distance between the two coherence peaks is around 33 meV, which gives a large $2\Delta_{SDW}/k_BT_{SDW} = 9.5$.

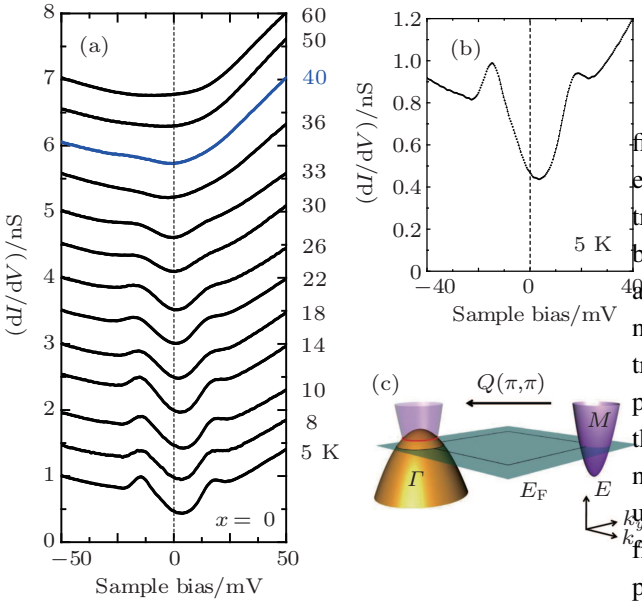


Fig. 3. The dI/dV spectroscopy of parent NaFeAs. (a) dI/dV spectra taken at various temperatures. The SDW gap closes at $T_{SDW} = 40$ K. (b) Spatially averaged dI/dV spectra taken at 5 K. A particle–hole asymmetric gap opens at E_F. (c) Schematic showing band crossing for electron–hole inter-FS scattering along (π, π) wave vector in folded Brillouin zone notation.[10]

We further explore the spatial dependence of the SDW gap in the parent compound. Figure 4(b) is a line-cut dI/dV spectroscopy taken along the red line indicated in Fig. 4(a). Although the topography of Fig. 4(a) shows NaFeAs surface with multiple defects, the dI/dV spectroscopy displays a spatially uniform single SDW gap.

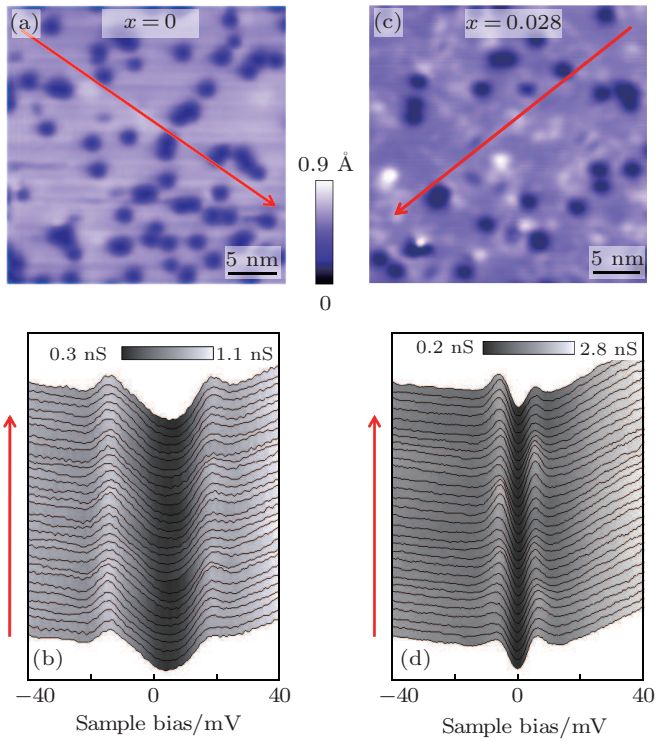


Fig. 4. Spatial dependence of both SDW and SC gap. (a) Constant current image of cleaved parent NaFeAs surface. (b) Line-cut dI/dV spectra taken along the red line shown in panels (a), displaying spatially uniform SDW gap. (c) Topography of optimally doped $x = 0.028$ sample, showing more disorder due to Co doping. (d) Line-cut dI/dV spectra taken on the optimally doped sample along the red line shown in panel (c), presenting a particle–hole symmetric SC gap with negligible spatial dependence.[11]

The direct observation of an SDW gap in NaFeAs confirms that its cleaved surface reflects the intrinsic bulk properties. An interesting structure revealed by our dI/dV spectroscopy is the asymmetric feature of the SDW gap, which can be understood in the FS nesting picture. Figure 3(c) shows a cartoon, which illustrates the nesting wave vector that connects the hole pocket and the electron pocket. When the electron pocket is shifted along the (π, π) direction to the hole pocket, it may intersect at an energy deviated from E_F, where the gap opens. Since the hole and electron pockets are not necessarily symmetric with respect to E_F, this asymmetry naturally leads to an asymmetric gap with the bottom deviated from E_F. In the nesting picture, the gap opens at the nested portions of the FS and leaves the other part unaffected, which explains the residual DOS at E_F. Although the existence of an SDW gap supports the itinerant point of view regarding the nature of magnetic order in the parent phase, we note that a pure itinerant picture is not enough. In a pure itinerant system,

the SDW wave vector is exclusively determined by the FS geometry, thus the SDW wave vector is usually incommensurate and may change with temperature. A well-known example is Cr, whose SDW wave vector undergoes complex evolution with temperature.[27] In NaFeAs, on the other hand, the SDW wave vector is always commensurate at (π, π), which is the characteristic wave vector of the magnetic correlation of the local moments in the parent compound. Recent magnetization measurement on NaFeAs shows a linear temperature dependence of magnetic susceptibility, indicating the existence of local moments.[21] As more experimental data are accumulated, it becomes more evident that the itinerant electrons and local moments should be treated on an equal footing. They both exist in the system, and are coupled to each other via the Hund's rule coupling J. It is the cooperation of itinerant electrons and local moments that finally drives a commensurate SDW order in the parent phase.[28,29]

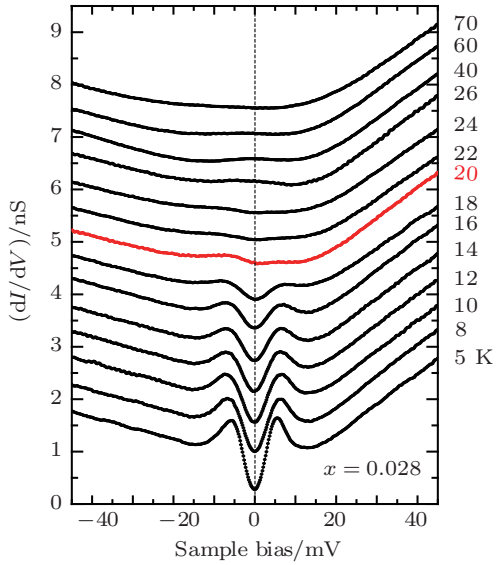


Fig. 5. Varied-T $\mathrm{d}I/\mathrm{d}V$ spectroscopy measurement of optimally doped $NaFe_{0.972}Co_{0.028}As$ sample. A particle–hole symmetric SC gap closes at $T_c = 20$ K with a featureless normal state spectrum.[10]

4. SC gap in the optimally doped regime

Cobalt doping suppresses the SDW order and induces bulk superconductivity in $NaFe_{1-x}Co_xAs$. A maximum $T_c = 20$ K occurs at $x = 0.028$, so $NaFe_{0.972}Co_{0.028}As$ is optimally doped. Figure 5 shows the $\mathrm{d}I/\mathrm{d}V$ spectroscopy taken at 5 K. In contrast to the SDW gap found in the parent phase, here we see a particle–hole symmetric gap with the gap bottom right at E_F. The varied-T measurement in Fig. 5 confirms its SC gap origin. The SC gap size 2Δ determined from the distance between the two coherence peaks is 11 meV, which gives the ratio $2\Delta/k_BT_c = 6.4$, close to previous STM study on other iron-based superconductors.[13] It is also consistent with recent ARPES measurements of the optimally doped $NaFe_{1-x}Co_xAs$.[30] Figure 4(d) is the line-cut $\mathrm{d}I/\mathrm{d}V$ spectroscopy taken along the red line shown in Fig. 4(c). Similar to the parent phase, it displays a spatially uniform single SC gap on the optimally doped $NaFe_{0.972}Co_{0.028}As$. A clear contrast to the SDW gap is the symmetric line shape of SC gap required by the particle–hole symmetry of Bogoliubov quasiparticles.

The weak spatial variation of SC gap spectrum is consistent with another STM study on a similar compound, which suggests that Co impurity acts as a very weak scattering center.[31] This observation is not trivial, since a magnetic impurity (such as Co, Ni) is usually expected to drastically affect the SC. A previous STM study on cuprates revealed a distinct Ni impurity state in the SC gap spectrum. However, the absence of a Co-related impurity state in $NaFe_{1-x}Co_xAs$ calls for close examination. As discussed in Ref. [31], the Co impurity may behave as an extended scattering center, thus does not affect the electron and hole inter-FS scattering (if it would be the cause of SC pairing). Therefore, it has a negligible effect on the SC gap spectrum.

5. Microscopic coexistence of SDW and SC order in the underdoped regime

The distinct features of SDW and SC gap in $\mathrm{d}I/\mathrm{d}V$ spectroscopy serve as fingerprints for each order. Now we are ready to explore their relationship in the underdoped regime. More precisely, we want to find out whether SDW and SC orders can microscopically coexist in real space or must exclude each other. Many experiments and theories have concentrated on this question in iron-based superconductors. In $LaO_{1-x}F_xFeAs$, muon spin relaxation (μSR) and Mössbauer spectroscopy suggest a first-order-like transition from SDW to SC without coexistence.[32] On the contrary, μSR and neutron scattering in $BaFe_{2-x}Co_xAs_2$ reveal the coexistence of two phases.[33,34] The STM can detect a material's electronic structure down to atomic scale and thus is an ideal probe to resolve the controversy regarding the relationship between SDW and SC in the underdoped regime.

We use line-cut spectroscopy to reveal the electronic structure in the underdoped $NaFe_{0.986}Co_{0.014}As$ sample surface, as shown in Figs. 6(b)–6(d). The line-cut at 5 K displays more pronounced spatial variations, as compared to the parent and optimally doped phases. In addition, two-gap feature can be discerned in each $\mathrm{d}I/\mathrm{d}V$ curve of the line-cut. The larger gap has a peak at -17 mV, and the smaller one has a kink at -5 mV. On the positive side, however, the coherent peak positions are not well separated. To identify the origin of these two gaps, we conduct the varied-T measurement. Figures 6(c) and (d) are two line-cuts taken at the same locations as Fig. 6(b), but at $T = 10$ K and 16 K respectively. One can see that the small gap disappears at $T_c = 16$ K, indicating its SC gap origin. The large particle–hole asymmetric gap remains at 16 K. It disappears as the temperature increases to above $T_{SDW} = 22$ K

(see Fig. 6(e)). Thus, the large gap can be safely attributed to the SDW order. The SDW gap size, determined by the distance between two coherence peaks, is $\Delta_{\rm SDW} = 26$ meV in the underdoped sample, smaller than that of parent compound. There is also a large residual DOS around $E_{\rm F}$ after the SDW gap opens. Since we observe both the SDW and SC gaps at the same location, it unambiguously demonstrates the microscopic coexistence of SDW and SC orders in the underdoped regime. We can also extract the SC gap signal from the SDW gap background by normalizing the 5 K line-cut, as shown in Figs. 7(a) and 7(b). All the $\mathrm{d}I/\mathrm{d}V$ spectra in the line-cut are taken at the same locations as temperature increases. This atomic registration justifies such normalization. The normalized line-cut clearly shows a spatially uniform particle–hole symmetric SC gap, whose size is $\Delta_{\rm SC} = 10$ meV and gradually shrinks as temperature increases to $T_{\rm c}$. Thus, the SC state is everywhere, which excludes the phase separation and further corroborates the microscopic coexistence of SDW and SC.

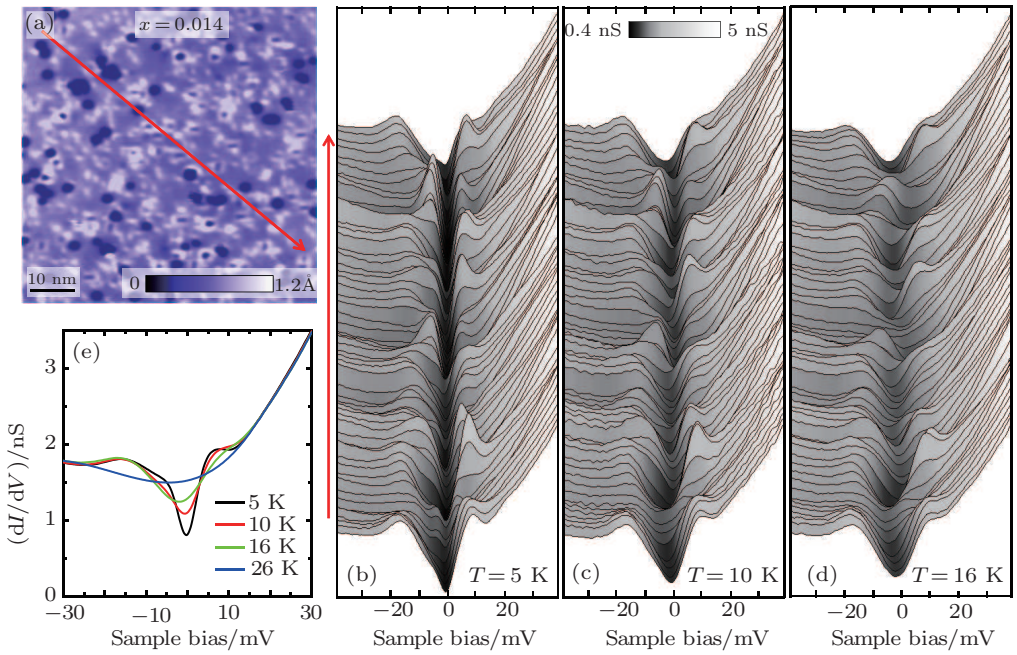


Fig. 6. The $\mathrm{d}I/\mathrm{d}V$ spectroscopy of underdoped $NaFe_{0.986}Co_{0.014}As$ sample. (a) Topography of underdoped sample on a large area. (b) Line-cut $\mathrm{d}I/\mathrm{d}V$ spectra taken at 5 K along the red line shown in panel (a). It displays more complex structure than the parent and optimally doped phases. Two-gap features can be seen on each $\mathrm{d}I/\mathrm{d}V$ curve, together with strong spatial variations. (c, d) The same line-cut $\mathrm{d}I/\mathrm{d}V$ spectra taken at 10 K and 16 K, respectively. The small SC gap feature around $E_{\rm F}$ gradually diminishes as T increases to $T_{\rm c} = 16$ K. However, the large asymmetric SDW gap remains above $T_{\rm c}$ and shows strong spatial variations. (e) The spatially-averaged $\mathrm{d}I/\mathrm{d}V$ spectra taken at various temperatures show the evolution from the two-gap features at 5 K to a single SDW gap at $T_{\rm c}$, and a gapless normal state above $T_{\rm SDW} = 22$ K.[11]

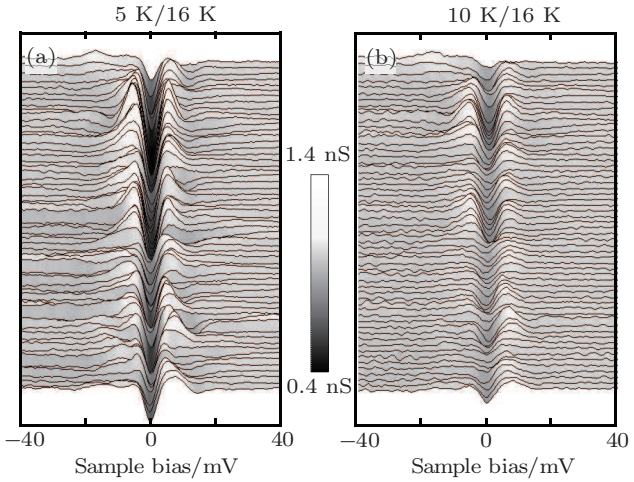


Fig. 7. Normalized $\mathrm{d}I/\mathrm{d}V$ spectra of underdoped $NaFe_{0.986}Co_{0.014}As$ sample. (a) and (b) $\mathrm{d}I/\mathrm{d}V$ spectra taken at 5 K and 10 K are divided by that taken at $T_{\rm c} = 16$ K. The SC gap can be extracted by such normalization. It shows a spatially uniform particle–hole symmetric SC gap.[11]

Now that the microscopic coexistence of SDW and SC is unambiguously established, the next question is the interplay between them. The strong spatial variations in $\mathrm{d}I/\mathrm{d}V$, as shown in Fig. 6(b), already makes clear contrast to the spatially uniform spectra in both parent and optimally doped phases. Figure 8(a) shows five typical $\mathrm{d}I/\mathrm{d}V$ curves selected from the 5-K line-cut in Fig. 6(b). The conductance value at the SC peak at -5 mV and the SDW peak at -17 mV roughly indicates the local SC/SDW order strength. It immediately shows that when the SC strength gets weaker, the SDW strength becomes stronger, and vice versa. This trend indicates a competition between SC and SDW, which is clearly demonstrated by the anti-correlation of the SDW peak conductance against SC peak conductance plotted in Fig. 8(b). To directly visualize this competition in real space, a conductance map is performed at -5 mV and -17 mV in Figs. 8(c) and 8(d) to

show the spatial dependence of relative SC and SDW strength in the same area. Disregarding some sparse impurity states, we find that the areas with relatively weak SC strength show relatively strong SDW strength, and vice versa. Thus, the competition between SC and SDW is clearly visualized by such conductance mapping.

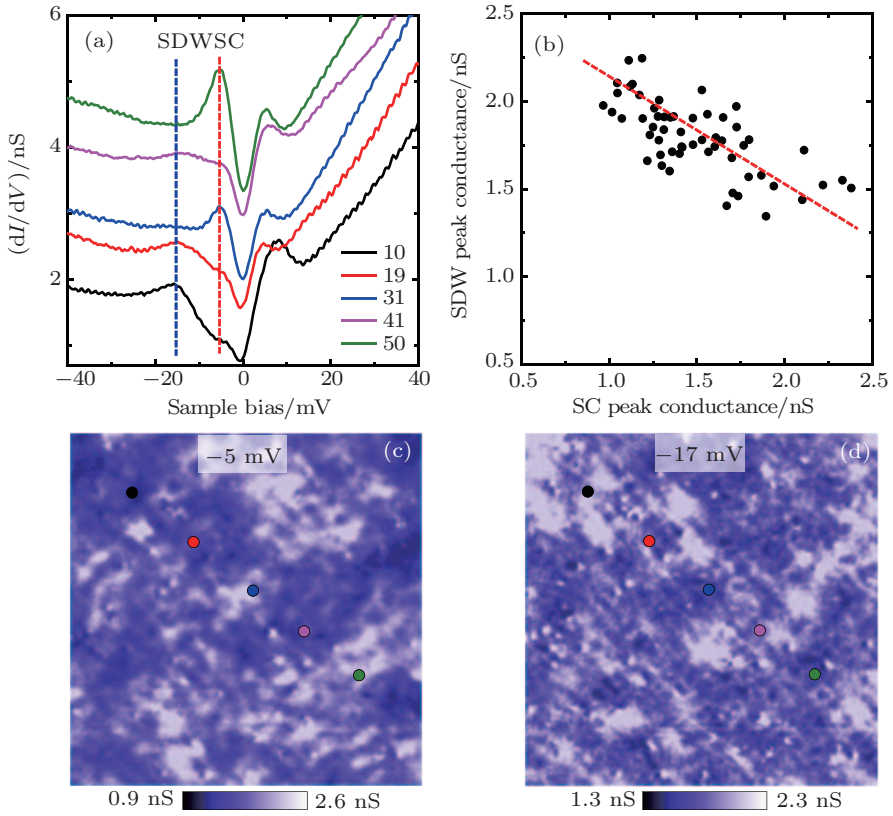


Fig. 8. Anti-correlation between SDW and SC features in underdoped $NaFe_{0.986}Co_{0.014}As$ sample. (a) Five dI/dV spectra selected from the line-cut in Fig. 6(b). Both SDW and SC gap features are pronounced at the negative bias, with the SDW coherence peak at −17 mV and SC gap feature at −5 mV. (b) Plot of conductance value at the SDW peak −17 mV as a function of conductance at SC peak −5 mV, displaying clear anti-correlation. (c) and (d) Conductance maps at −17 mV and −5 mV on the same field of view, presenting the spatial dependence of relative SDW- and SC-order strengths, and showing anti-correlation between them.[11]

The direct visualization of microscopic coexistence of SDW and SC and their competition puts strong constraints on the theoretical models for the iron-based superconductors. ARPES measurements of a similar compound confirm this observation.[35] The usual reason for not believing the coexistence of a density wave order and superconductivity is that once the former gaps the FS, the susceptibility toward Cooper pairing is strongly suppressed. Our finding forces us to reconsider this picture. A more reasonable picture in $NaFe_{1-x}Co_xAs$ is that the SDW and SC can coexist in real space, but compete for the FS in k-space. Once the SDW order gaps the nested part of the FS, the Cooper pairs have to be developed at the un-gapped residual FS.

6. Pseudogap-like feature in the overdoped regime

We study two overdoped samples: $NaFe_{0.939}Co_{0.061}As$ (T_c = 13 K) and $NaFe_{0.925}Co_{0.075}As$ (T_c = 11 K). Our dI/dV spectroscopy reveals an unexpected feature in the normal state in the overdoped regime: a pseudogap-like structure around E_F. Figure 9(a) shows the dI/dV spectra of $NaFe_{0.939}Co_{0.061}As$ taken at various temperatures up to 70 K. Below T_c, an SC gap opens at E_F. As the temperature increases and passes T_c, the gap is gradually filled up and the coherence peak at the positive side diminishes, corresponding to an SC gap closure. Above T_c, there is still a sizable DOS suppression at E_F. Such suppression forms an asymmetric pseudogap-like structure in the normal state, with a hump feature at the negative side. As we continue to raise the temperature, this pseudogap-like feature is weakened, and finally disappears at around 55 K. $NaFe_{0.925}Co_{0.075}As$ behaves similarly, as shown in Fig. 9(b).

We gain more insights into this pseudogap-like phase by taking advantage of the spatial resolution of STM. Figure 10(a) is the topography of $NaFe_{0.939}Co_{0.061}As$. We draw a line-cut on it and take dI/dV spectra at multiple points along the line-cut. Figure 10(b) shows the line-cut spectra taken at 5 K. Figure 10(c) is taken at 16 K, which is above T_c = 13 K. We note that both line-cut spectra are taken at the same spots, so they can be directly compared to each other. The feature at two energy scales can be discerned, especially from the red dI/dV curve in Fig. 10(b). Two symmetric kinks reside near

E_F and disappear above T_c, thus corresponding to the SC gap edges. A hump feature at higher energy is located at the negative side. It persists to temperatures above T_c, and gives rise to the pseudogap-like structure in the normal state. We note that such a pseudogap-like feature also displays strong spatial variations, as seen in Fig. 10(c). The SC gap information can be extracted from the normalized line-cut spectroscopy, as shown in Fig. 10(d). This shows that the SC gap is particle–hole symmetric and spatially uniform, in sharp contrast to the highly asymmetric and spatially varied pseudogap-like feature.

A close analogy can be drawn between our finding here and the pseudogap in the underdoped cuprates, where a small, spatially uniform SC gap coexists with a large, spatially varied pseudogap.[36,37] Interestingly, both the SC gap and pseudogap-like feature disappear all together in the extremely overdoped non-SC regime ($x = 0.109$), which indicates a close relationship between them.[10]

The observed pseudogap-like feature represents a new electronic structure in the $NaFe_{1-x}Co_xAs$ phase diagram. At first sight, its temperature evolution (see Fig. 9), together with the asymmetric line shape, closely mimics the SDW gap in the parent phase. They both coexist with SC and survive above T_c. However, the strong spatial variation makes it very different from the spatially uniform SDW gap. The exact nature of this pseudogap-like feature deserves further investigation.

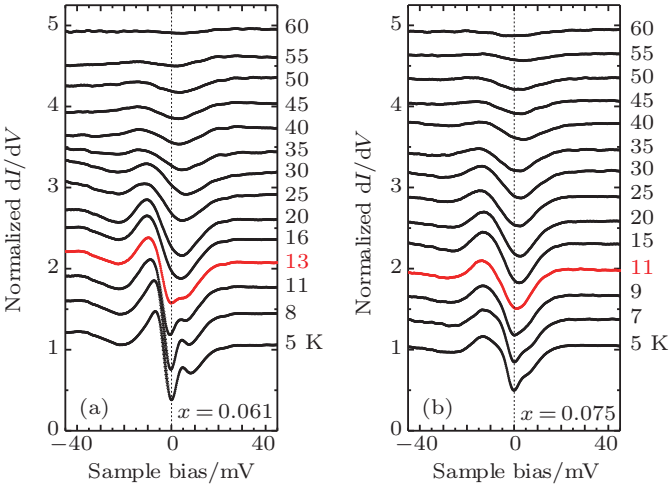


Fig. 9. The dI/dV spectroscopy of overdoped $NaFe_{1-x}Co_xAs$ sample. (a, b) Varied-T dI/dV spectra of two overdoped $NaFe_{0.939}Co_{0.061}As$ and $NaFe_{0.925}Co_{0.075}As$ samples. A large asymmetric gap feature coexists with the SC gap below T_c and persists well into the normal state.[10]

7. Anomalous high-energy electronic structure

The high-energy electronic structure of $NaFe_{1-x}Co_xAs$ can be probed by the dI/dV spectroscopy in a large energy window. Figure 11(a) shows dI/dV taken at ± 500 meV energy range for various doping levels in $NaFe_{1-x}Co_xAs$. The most pronounced feature here is a large V-shaped DOS suppression around E_F. It exists in the phase diagram and is independent of temperature. The bottom of DOS is located at E_F.

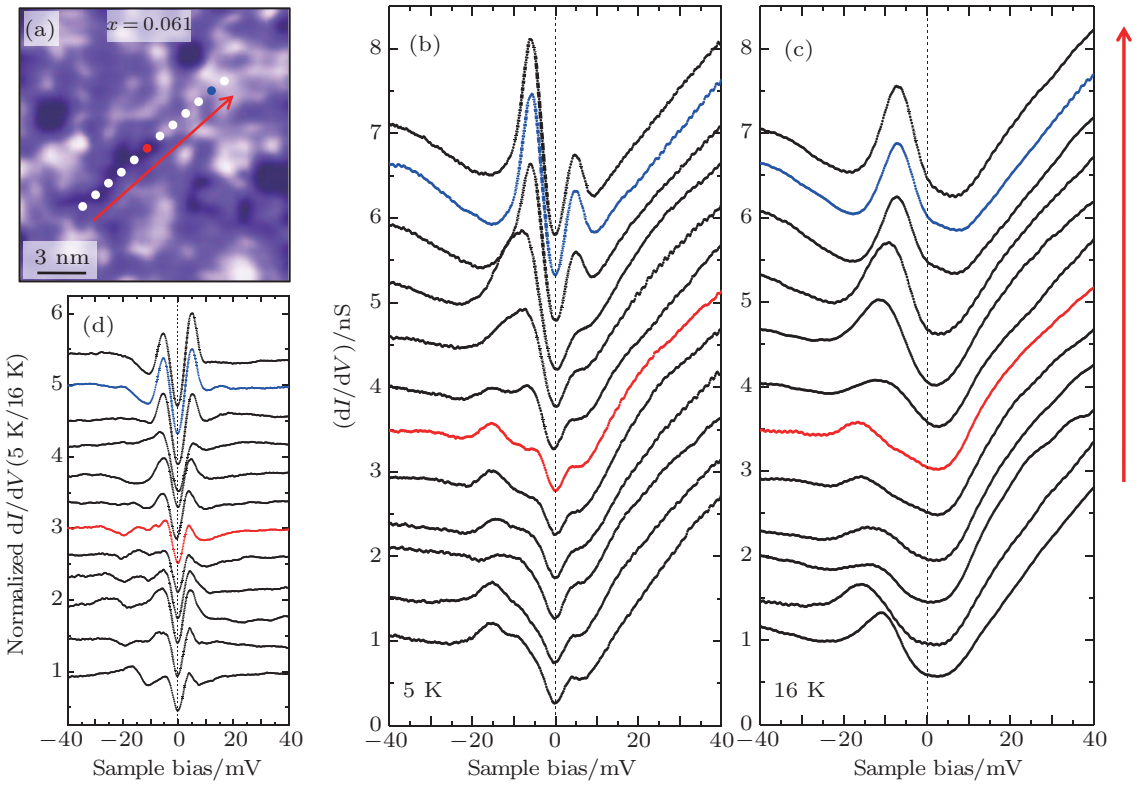


Fig. 10. Spatial dependence of dI/dV spectroscopy of overdoped $NaFe_{0.939}Co_{0.061}As$ sample. (a) Topography of overdoped $NaFe_{0.939}Co_{0.061}As$ sample. (b) and (c) Line-cut dI/dV spectra taken at 5 K and 16 K respectively along the red line shown in panel (a). A large asymmetric gap coexists with SC gap and survives above $T_c = 13$ K. It also displays strong spatial dependence. (d) Normalized 5-K line-cut dI/dV spectroscopy, showing spatially uniform SC gap.[10]

As we dope the system with Co, this large V-shaped structure does not move as expected in a rigid band picture. Instead, its bottom is pinned at E_F. Only when we reach the extremely overdoped non-SC regime ($x = 0.109$), does the overall structure suddenly shift to the negative side. This behavior is certainly incompatible with a rigid band model.

The anomalous high-energy V-shaped structure and its peculiar doping evolution call for new theoretical insights. We argue that a local-itinerant coexistent model is needed to consistently explain it. Initial theoretical work has already emphasized the dual role played by the Fe 3d electrons, wherein some of them undergo a selective Mott transition.[38] They are localized and contribute to the local moments, and the remaining 3d electrons are delocalized and constitute the itinerant part. The two degrees of freedom are coupled to each other via the Hund's rule coupling J. Figure 11(b) shows a schematic electronic structure for such a local-itinerant coexistent model following Ref. [28]. In this model, the electronic DOS consists of two parts. The localized electrons will form a Mott-like gap, and the local moment is contributed by a filled lower Hubbard band. The itinerant electrons provide the extra DOS at E_F. Thus, the V-shaped electronic structure in our dI/dV spectroscopy mimics such Mott-like gap, and the residual DOS at E_F comes from the itinerant part. Initial doping into the itinerant band will leave the large Mott-like gap intact and the gap bottom pinned at E_F until the upper Hubbard band starts to get filled at strong overdoping, which results in a sudden jump at $x = 0.109$.

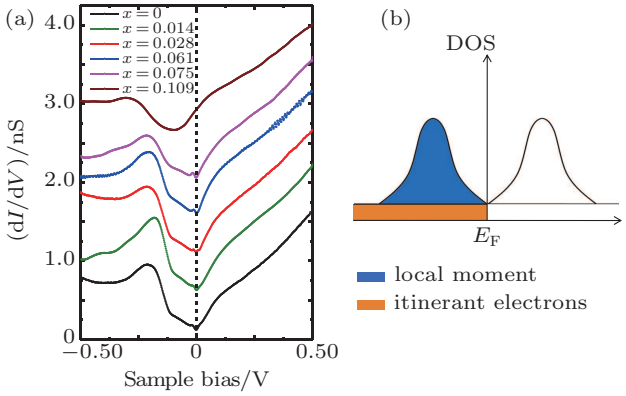


Fig. 11. High energy dI/dV spectra of $NaFe_{1-x}Co_xAs$. (a) 5-K dI/dV spectra of $NaFe_{1-x}Co_xAs$ taken between ±500 meV, showing a large V-shaped feature for varied Co dopings. The bottom of DOS is pinned at E_F until the extremely overdoped non-SC regime ($x = 0.109$). (b) Schematic plot of the electronic DOS based on the itinerant-localized hybrid model.[10]

8. Conclusions and perspectives

Our STM studies on the $NaFe_{1-x}Co_xAs$ phase diagram reveal rich electronic structures and their doping evolution. The complex variations of low-energy electronic states, especially the observed SDW gap in the parent phase, demonstrate the significant role played by the itinerant electrons. On the other hand, the anomalous high-energy electronic feature and its doping evolution underline the existence of local moments in the system. These observations put strong constraints on the theoretical models for the iron-based superconductors. We argue that a realistic model should treat the itinerant electrons and local moments on an equal footing. In essence, this dichotomy comes from the fact that the iron-based superconductors reside in the intermediate region of Hubbard U/W couplings, where the coupling is neither very weak (in which case the itinerant picture would apply) nor very strong (in which case the localized Mott physics would dominate). A still better understanding of iron-based superconductors will require a meticulous treatment of the degree of itinerancy, which varies in different iron-based superconductor systems. Recent neutron and ARPES measurements also support the coexistence of these two degrees of freedom.[39,40]

The nature of the pseudogap-like phase in the overdoped regime may be explained within the same picture. Based on our STM data, the significant spatial variation may indicate its local origin. The asymmetric line shape of the pseudogap-like feature reminds us of the Fano resonance in Kondo physics, where the local moments and itinerant electrons are antiferromagnetically coupled to each other.[41] Because in iron-based superconductors, the Hund's rule coupling J is ferromagnetic, we speculate that the pseudogap-like phase might be a manifestation of a ferromagnetic version of "Kondo-like" physics. Of course, more experimental results and theoretical considerations are needed to eventually clarify its origin.

Acknowledgments

We thank Ruan Wei and Ye Cun for assistance in experiments, You Yi-Zhuang, Weng Zheng-Yu, and Lee Dung-Hai for helpful theoretical discussions. Wang Ai-Feng and Chen Xian-Hui provided all the $NaFe_{1-x}Co_xAs$ single crystals studied here.

References

[1] Kamihara Y, Watanabe T, Hirano M and Hosono H 2008 *J. Am. Chem. Soc.* **130** 3296
[2] Chubukov A V, Efremov D V and Eremin I 2008 *Phys. Rev. B* **78** 134512
[3] Mazin I I, Singh D J, Johannes M D and Du M H 2008 *Phys. Rev. Lett.* **101** 057003
[4] Si Q M and Abrahams E 2008 *Phys. Rev. Lett.* **101** 076401
[5] Seo K J, Bernevig B A and Hu J P 2008 *Phys. Rev. Lett.* **101** 206404
[6] Wang F, Zhai H, Ran Y, Vishwanath A and Lee D H 2009 *Phys. Rev. Lett.* **102** 047005
[7] de la Cruz C, Huang Q, Lynn J W, Li J Y, Ratcliff W, Zarestky J L, Mook H A, Chen G F, Luo J L, Wang N L and Dai P C 2008 *Nature* **453** 899
[8] Dong J, Zhang H J, Xu G, Li Z, Li G, Hu W Z, Wu D, Chen G F, Dai X, Luo J L, Fang Z and Wang N L 2008 *Europhys. Lett.* **83** 27006
[9] Haule K and Kotliar G 2009 *New J. Phys.* **11** 025021
[10] Zhou X D, Cai P, Wang A F, Ruan W, Ye C, Chen X H, You Y Z, Weng Z Y and Wang Y Y 2012 *Phys. Rev. Lett.* **109** 037002

[11] Cai P, Zhou X D, Ruan W, Wang A F, Chen X H, Lee D H and Wang Y Y 2013 *Nat. Commun.* **4** 1596

[12] Fischer O, Kugler M, Maggio-Aprile I, Berthod C and Renner C 2007 *Rev. Mod. Phys.* **79** 353

[13] Hoffman J E 2011 *Rep. Prog. Phys.* **74** 124513

[14] Yin Y, Zech M, Williams T L, Wang X F, Wu G, Chen X H and Hoffman J E 2009 *Phys. Rev. Lett.* **102** 097002

[15] Nascimento V B, Li A, Jayasundara D R, Xuan Y, O'Neal J, Pan S H, Chien T Y, Hu B, He X B, Li G R, Sefat A S, McGuire M A, Sales B C, Mandrus D, Pan M H, Zhang J D, Jin R and Plummer E W 2009 *Phys. Rev. Lett.* **103** 076104

[16] Chuang T M, Allan M P, Lee J, Xie Y, Ni N, Bud'ko S L, Boebinger G S, Canfield P C and Davis J C 2010 *Science* **327** 181

[17] Zhang H, Dai J, Zhang Y J, Qu D R, Ji H W, Wu G, Wang X F, Chen X H, Wang B, Zeng C G, Yang J L and Hou J G 2010 *Phys. Rev. B* **81** 104520

[18] Zhou X D, Ye C, Cai P, Wang X F, Chen X H and Wang Y Y 2011 *Phys. Rev. Lett.* **106** 087001

[19] Hanaguri T, Niitaka S, Kuroki K and Takagi H 2010 *Science* **328** 474

[20] Allan M P, Rost A W, Mackenzie A P, Xie Y, Davis J C, Kihou K, Lee C H, Iyo A, Eisaki H and Chuang T M 2012 *Science* **336** 563

[21] Wang A F, Luo X G, Yan Y J, Ying J J, Xiang Z J, Ye G J, Cheng P, Li Z Y, Hu W J and Chen X H 2012 *Phys. Rev. B* **85** 224521

[22] Zhao J, Adroja D T, Yao D X, Bewley R, Li S L, Wang X F, Wu G, Chen X H, Hu J P and Dai P C 2009 *Nat. Phys.* **5** 555

[23] Li S L, de la Cruz C, Huang Q, Chen Y, Lynn J W, Hu J P, Huang Y L, Hsu F C, Yeh K W, Wu M K and Dai P C 2009 *Phys. Rev. B* **79** 054503

[24] Dagotto E 2012 arXiv: 1210.6501 [cond-mat.supr-con]

[25] Li S L, de la Cruz C, Huang Q, Chen G F, Xia T L, Luo J L, Wang N L and Dai P C 2009 *Phys. Rev. B* **80** 020504

[26] Hu W Z, Li G, Zheng P, Chen G F, Luo J L and Wang N L 2009 *Phys. Rev. B* **80** 100507

[27] Fawcett E 1988 *Rev. Mod. Phys.* **60** 209

[28] Kou S P, Li T and Weng Z Y 2009 *Europhys. Lett.* **88** 17010

[29] You Y Z, Yang F, Kou S P and Weng Z Y 2011 *Phys. Rev. B* **84** 054527

[30] Liu Z H, Richard P, Nakayama K, Chen G F, Dong S, He J B, Wang D M, Xia T L, Umezawa K, Kawahara T, Souma S, Sato T, Takahashi T, Qian T, Huang Y B, Xu N, Shi Y B, Ding H and Wang S C 2011 *Phys. Rev. B* **84** 064519

[31] Yang H, Wang Z Y, Fang D L, Li S, Kariyado T, Chen G F, Ogata M, Das T, Balatsky A V and Wen H H 2012 *Phys. Rev. B* **86** 214512

[32] Luetkens H, Klauss H H, Kraken M, Litterst F J, Dellmann T, Klingeler R, Hess C, Khasanov R, Amato A, Baines C, Kosmala M, Schumann O J, Braden M, Hamann-Borrero J, Leps N, Kondrat A, Behr G, Werner J and Buchner B 2009 *Nat. Mater.* **8** 305

[33] Pratt D K, Tian W, Kreyssig A, Zarestky J L, Nandi S, Ni N, Bud'ko S L, Canfield P C, Goldman A I and McQueeney R J 2009 *Phys. Rev. Lett.* **103** 087001

[34] Marsik P, Kim K W, Dubroka A, Roessle M, Malik V K, Schulz L, Wang C N, Niedermayer C, Drew A J, Willis M, Wolf T and Bernhard C 2010 *Phys. Rev. Lett.* **105** 057001

[35] Ge Q Q, Ye Z R, Xu M, Zhang Y, Jiang J, Xie B P, Song Y, Zhang C L, Dai P and Feng D L 2013 *Phys. Rev. X* **3** 011020

[36] McElroy K, Lee D H, Hoffman J E, Lang K M, Lee J, Hudson E W, Eisaki H, Uchida S and Davis J C 2005 *Phys. Rev. Lett.* **94** 197005

[37] Boyer M C, Wise W D, Chatterjee K, Yi M, Kondo T, Takeuchi T, Ikuta H and Hudson E W 2007 *Nat. Phys.* **3** 802

[38] de' Medici L, Hassan S R and Capone M 2009 *J. Supercond. Nov. Magn.* **22** 535

[39] Richard P, Sato T, Nakayama K, Takahashi T and Ding H 2011 *Rep. Prog. Phys.* **74** 124512

[40] Dai P C, Hu J P and Dagotto E 2012 *Nat. Phys.* **8** 709

[41] Madhavan V, Chen W, Jamneala T, Crommie M F and Wingreen N S 1998 *Science* **280** 567